SeaWiFS on-orbit gain and detector calibrations: effect on ocean products

Robert E. Eplee, Jr.,[1,*] Frederick S. Patt,[1] Bryan A. Franz,[1] Sean W. Bailey,[2] Gerhard Meister,[2] and Charles R. McClain[3]

[1]Science Applications International Corporation, 4600 Powder Mill Road, Suite 400, Beltsville, Maryland 20705, USA
[2]Futuretech Corporation, 7307 Hanover Parkway, Suite D, Greenbelt, Maryland 20770, USA
[3]Ocean Biology Processing Group, Mail Code 614.8, NASA Goddard Space Flight Center, Greenbelt, Maryland 20771, USA

*Corresponding author: Robert.E.Eplee@nasa.gov

Received 17 April 2007; revised 12 July 2007; accepted 20 July 2007; posted 24 July 2007 (Doc. ID 82156); published 12 September 2007

The NASA Ocean Biology Processing Group's Calibration and Validation Team has analyzed the mission-long Sea-Viewing Wide Field-of-View Sensor (SeaWiFS) on-orbit gain and detector calibration time series to verify that lunar calibrations, obtained at nonstandard gains and radiance ranges, are valid for Earth data collected at standard gains and typical ocean, cloud, and land radiances. For gain calibrations, a constant voltage injected into the postdetector electronics allows gain ratios to be computed for all four detectors in each band. The on-orbit lunar gain ratio time series show small drifts for the near infrared bands. These drifts are propagated into the ocean color data through the atmospheric correction parameter ϵ, which uses the 765/865 nm band ratio. An anomaly analysis of global mean normalized water-leaving radiances at 510 nm shows a small decrease over the mission, while an analysis of ϵ shows a corresponding increase. The drifts in the lunar time series for the 765 and 865 nm bands were corrected. An analysis of the revised water-leaving radiances at 510 nm shows the drift has been eliminated, while an analysis of ϵ shows a reduced drift. For detector calibrations, solar diffuser observations made by the individual detectors in each band allows the response of the detectors to be monitored separately. The mission-long time series of detector calibration data show that the variations in the response of the individual detectors are less than 0.5% over the mission for all bands except the 865 nm band, where the variations are less than 1%. © 2007 Optical Society of America

OCIS codes: 280.0280, 010.0010, 010.4450, 120.0120, 120.5630, 120.0280.

1. Introduction

The Sea-viewing Wide Field-of-view Sensor (SeaWiFS) has been providing daily global imagery of the world's oceans since September 1997. The goal of the NASA Ocean Biology Processing Group's (OBPG's) Calibration and Validation (Cal/Val) Team is to produce a long-term ocean color data set with 5% absolute and 1% relative accuracies for the water-leaving radiances and 35% accuracy for chlorophyll a concentrations in open-ocean regions [1]. To meet this goal, the Cal/Val Team has implemented an on-orbit calibration strategy that uses monthly lunar calibrations to monitor the radiometric stability of the instrument over its mission lifetime and that uses daily solar calibration to look for short-period, step-function changes in the instrument response [2,3]. The Cal/Val Team has also used data from the NASA/NOAA Marine Optical Buoy (MOBY) to vicariously calibrate the integrated instrument and atmospheric correction algorithm system [4,5]. The implementation of this calibration strategy requires the on-orbit calibration of the commanded gains of the instrument and of the individual detectors within each band. The Cal/Val Team initially described these two on-orbit calibrations four years into the SeaWiFS mission [6]. This paper describes how the strategy has evolved since that time.

SeaWiFS, having completed the tenth year of its mission, provides the Earth remote sensing community with the opportunity to understand how sensors

0003-6935/07/276733-18$15.00/0
© 2007 Optical Society of America

Table 1. SeaWiFS Bands

Band	Wavelength[a]	Bandwidth[a]
1	412	20
2	443	20
3	490	20
4	510	20
5	555	20
6	670	20
7	765	40
8	865	40

[a]The nominal center wavelengths and bandwidths are in nanometers.

perform on orbit over such long mission periods. The SeaWiFS experience highlights the importance of mission-long on-orbit calibration and validation data sets to the generation and maintenance of a long-term, climate-quality ocean color data set.

SeaWiFS is an eight-band visible and near-infrared (NIR) scanning radiometer designed to have high radiometric sensitivity over oceans without saturating over bright clouds. The bands are provided in Table 1. Each band is composed of three high sensitivity ocean detectors and one lower sensitivity cloud detector. For normal observations, the output from the four detectors in each band is averaged together on orbit, resulting in a bilinear response for each band of the instrument due to the saturation of the ocean detectors at high radiances. This bilinear response can be shown as a calibration curve, which gives the spectral radiances measured by SeaWiFS in terms of the signal from the instrument. The calibration curve for band 1 at the standard gain is shown in Fig. 1, where the slope of each segment is the counts-to-radiance conversion factor. The point at which each of the ocean detectors saturates is a knee in the bilinear response. The spectral radiances occur below the knee for ocean measurements and above the knee for cloud and land measurements. The bilinear response allows measurements of clouds or land to be made without saturating the instrument, thus allowing the ocean data to be corrected for stray light, allowing photosynthetically active radiation (PAR) to be computed over the spectral range of 400–700 nm, and allowing land measurements (normalized difference vegetation indices (NDVI) and surface reflectances) to be made at the radiometric sensitivity of the cloud detectors. This response has implications for the strategies implemented by the Cal/Val Team for the on-orbit calibration of SeaWiFS.

SeaWiFS obtains Earth measurements with detectors whose standard gains were optimized prior to launch for the expected typical top-of-the-atmosphere (TOA) radiances over the ocean in the visible (400–700 nm) and near-infrared (700–900 nm) bands. To keep the lunar and solar measurements below the knee of the bilinear response, the instrument electronics incorporate four commanded gains. Gain 1 is the standard gain for TOA radiances over the ocean. Gain 2 is the secondary gain for ocean observations

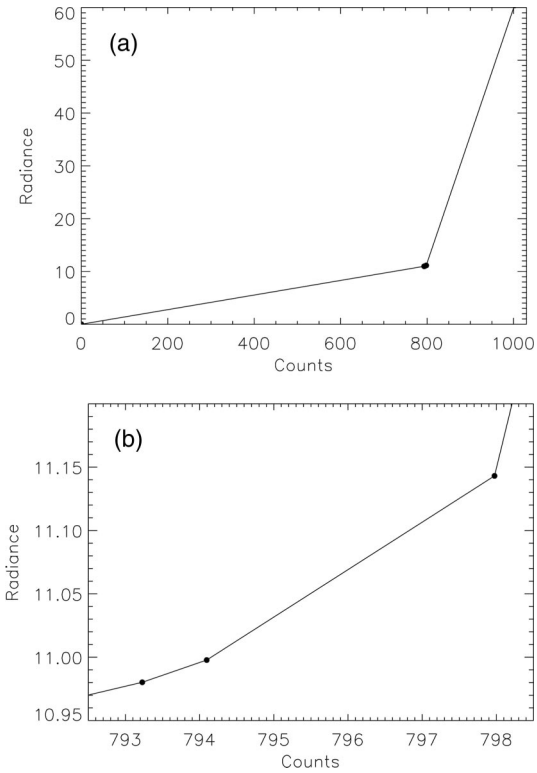

Fig. 1. Calibration curve for band 1 for the standard gain (Gain 1). (a) Measurements over the entire dynamic range of the band. (b) Measurements in the vicinity of the knees of the bilinear response. The radiance units are mW cm^{-2} sr^{-1} μm^{-1}.

(set at 2× the standard gain) designed to maintain the ocean color time series in the event of severe degradation of the radiometric response of a given band, and has yet to be used operationally. Gain 3 is a commanded gain set to give 3/4 full scale output from the instrument for lunar calibrations, while Gain 4 is a commanded gain set to give 3/4 full scale output for solar measurements. The gain settings for the cloud detectors cannot be changed on orbit. After the initial lunar and solar gains were defined, the optimum gains for those measurements were recomputed. The actual commanded gains used on-orbit for ocean, lunar, and solar measurements are shown in Table 2.

SeaWiFS is designed with two bands of four detectors, each on four separate focal planes. On each focal plane, the four detectors from each band are

Table 2. SeaWiFS Gains[a]

Target	Band 1	Band 2	Bands 3–8
Ocean	Gain 1	Gain 1	Gain 1
Lunar	Gain 4	Gain 3	Gain 3
Solar	Gain 3	Gain 1	Gain 3
2X	Gain 2	Gain 2	Gain 2

[a]Gain 1 is the standard gain for ocean observations. Gain 2 is the secondary gain (2×) for ocean observations. Gain 3 and Gain 4 are the commanded gains designed to give 3/4 full scale output for lunar and solar observations.

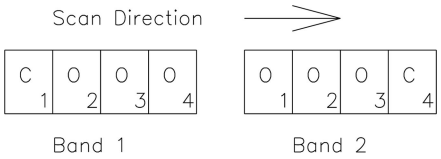

Fig. 2. Band 1/band 2 focal plane layout. The cloud (C) and ocean (O) detectors for each band are laid out as shown.

aligned in the along-scan direction and the two bands are located adjacent to each other, as is shown in Fig. 2 for the Band 1/Band 2 focal plane. For each focal plane, the two outside detectors (detector 1 for the odd-numbered bands and detector 4 for the even-numbered bands) are the cloud detectors and the interior detectors (detectors 2–4 for the odd-numbered bands and detectors 1–3 for the even-numbered bands) are the ocean detectors. For ocean, lunar, and solar observations, the outputs from the four detectors in each band are averaged using a time-delay-and-integration (TDI) technique to improve the signal-to-noise ratios [7]. The time delay is designed so that the output from each detector originates from the same pixel on the Earth's surface during the instrument scan. This mode of averaging the output from the four detectors in each band is referred to as the 4:1 TDI. For detector calibrations, observations are obtained in the 4:1 mode and in modes where measurements are made by the four individual detectors alone (TDI modes 1–4, corresponding to detectors 1–4). The Earth-observing mode of operation for SeaWiFS incorporates the standard gains (Gain 1) and the 4:1 TDI mode.

A. Lunar Calibration Background

The SeaWiFS on-orbit calibration strategy uses monthly lunar calibrations to monitor changes in the radiometric response of the instrument over its mission lifetime. The derivation of the lunar-based radiometric corrections is reviewed briefly here.

The Cal/Val Team has analyzed the mission-long SeaWiFS lunar calibration time series, encompassing 114 monthly lunar observations spanning some 3400 days from November 1997 through May 2007. During a lunar calibration the spacecraft is pitched across the Moon, so that SeaWiFS views the Moon near nadir through the same optical path as it views the Earth. The changes in radiometric response of the instrument are monitored through the same optical path as the Earth data are collected. The scan angles of the lunar observations are distributed over the range of $-15°$ to $+18°$, and the same scan modulation corrections are applied to both the lunar and Earth data. Consequently, the changes in the radiometric response of the instrument are independent of the angles of incidence of the lunar data [7]. The individual lunar observations have been normalized to a common viewing geometry for the radiometric stability analysis. Corrections computed from the time and geometry of the observations include Sun–Moon and instrument–Moon distances, oversampling of the lunar image (computed from the measured size of the lunar images in the along-track direction), and variations in the phase and libration angles of the Moon during the observations [3,8]. The lunar data incorporate the revised focal plane temperature correction coefficients for the period of 1 January 2006 onward [9]. The Cal/Val Team has fit the corrected lunar calibration time series by two simultaneous decaying exponential functions of time, with time constants of 200 and 2500 days, as shown in Fig. 3. The inverses of these fits constitute the radiometric corrections that are incorporated into the SeaWiFS calibration table.

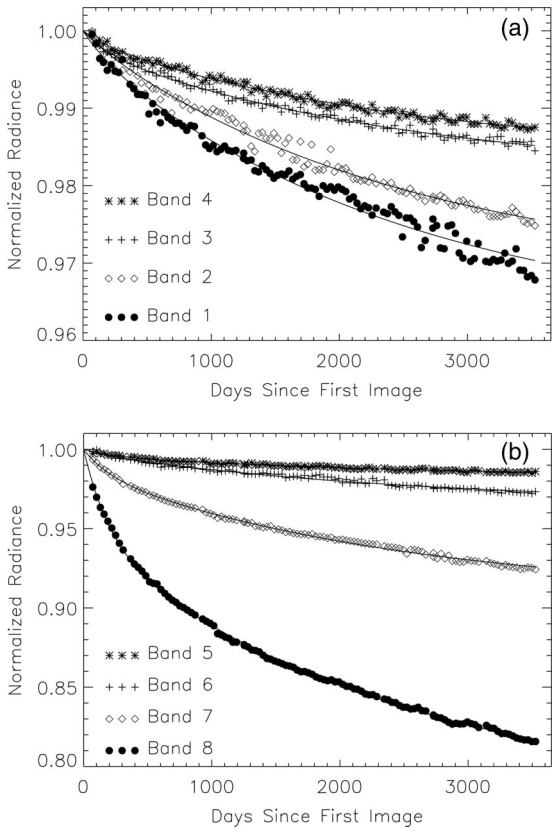

Fig. 3. Lunar calibration time series. The radiometric corrections contained in the calibration table are the inverses of the fits. The vertical scale of the plot for bands 1–4 in (a) is different from the vertical scale of the plot for bands 5–8 in (b).

B. Gain Calibration Rationale

Lunar radiances obtained at the standard gains would saturate the ocean detectors. Accordingly, the Cal/Val Team's on-orbit calibration strategy requires that changes in the radiometric response of the instrument, derived from lunar data obtained at the lunar commanded gains (Gain 3 or Gain 4), be applied to ocean data obtained at the standard gains (Gain 1). The prelaunch radiometric calibration of SeaWiFS provided counts-to-radiance conversion factors for each commanded gain [7]. Since changes in the radiometric response of a given band can vary as a function of commanded gain, the Cal/Val Team

must track possible gain variations by monitoring the temporal stability of gain ratios for each band. The stability of the gain ratios for each band is monitored on orbit by injecting a constant voltage signal (calibration pulse) into the postdetector electronics while stepping through the commanded gains for each of the detectors. The gain ratios (GR1, GR2, GR3, GR4) for a given band are defined relative to Gain 1 as follows:

$$\mathrm{GR}X(\lambda) = \frac{\mathrm{CP}(\mathrm{Gain}\ X,\ \lambda)}{\mathrm{CP}(\mathrm{Gain}\ 1,\ \lambda)}. \tag{1}$$

Here X designates the commanded gain (Gain 1, Gain 2, Gain 3, or Gain 4), λ designates the band, and CP(Gain X, λ) is the output counts from the band for a commanded gain, with the calibration pulse as input. Gain ratios are computed for individual detectors within a band in a similar manner. The gain calibrations are performed daily immediately following the solar calibrations, providing a time series of the gain ratios.

C. Detector Calibration Rationale

The Cal/Val Team's on-orbit calibration strategy also requires that changes in the instrument response derived from data obtained over low radiance ranges by all four detectors in each band (below the knee of the bilinear response) be applied to data obtained over high radiance ranges by the cloud detector alone (above the knee of the bilinear response). Consequently, the Cal/Val team must monitor the radiometric stability of the individual detectors within each band. The radiometric stability of the detectors in each band is monitored by solar calibrations that have been modified to collect data from each detector individually during the solar measurements. These detector calibrations are performed daily on the second orbit following the solar calibrations, providing a time series of the individual detector responses.

The components of the on-orbit calibration strategy, taken together, ensure that lunar calibrations, obtained at nonstandard gains and radiance ranges, are valid for Earth data collected at standard gains and typical ocean, cloud, and land radiance ranges. The following sections discuss the analyses of the mission-long gain and detector calibrations and the use of mission-long time series of global mean ocean color data products to validate the long-term stability of the on-orbit instrument calibration.

2. Prelaunch Gain Calibrations

The SeaWiFS design incorporates a zener diode for each band that provides a constant voltage source, or calibration pulse, for the postdetector electronics. During gain calibrations, the pulse is injected into the postdetector electronics. The mean calibration pulse at Gain 1 for each band during the prelaunch calibration is shown in Table 3. The gain calibration records the output from the four individual detectors in each band while the instrument cycles through the four gains and five TDI modes. In the analysis, the Cal/Val Team computes gain ratios for calibration pulse data obtained at Gain 2, Gain 3, and Gain 4 with calibration pulse data obtained at Gain 1 for each TDI mode. The calibration pulse was stable to better than a count throughout the prelaunch calibrations, though the gain ratio computations only require stability over a single gain calibration. Dur-

Table 3. SeaWiFS Calibration Pulse

Band	λ [nm]	Cal Pulse	σ(Cal Pulse)	Δ(Cal Pulse) (%)
1	412	384.13	±0.34	−0.69
2	443	380.98	±0.15	−1.8
3	490	365.74	±0.61	−1.0
4	510	364.00	±0.00	−1.6
5	555	363.95	±0.21	−2.3
6	670	361.92	±0.28	−1.1
7	765	351.06	±0.25	−1.6
8	865	371.72	±0.45	−1.1

[a]The values are given in counts. Δ(Cal Pulse) is the change in the calibration pulse over the mission.

Table 4. SeaWiFS Prelaunch Gain Ratios[a]

Band	Detector	GR1	GR2	GR3	GR4
1	1	1.0	1.016	1.005	1.010
	2	1.0	1.987	1.322	1.682
	3	1.0	1.982	1.317	1.678
	4	1.0	1.995	1.321	1.682
2	1	1.0	1.991	1.318	1.680
	2	1.0	1.983	1.320	1.682
	3	1.0	1.992	1.318	1.684
	4	1.0	1.024	1.008	1.016
3	1	1.0	1.051	1.000	1.038
	2	1.0	1.987	0.894	1.678
	3	1.0	1.989	0.897	1.684
	4	1.0	1.991	0.896	1.681
4	1	1.0	1.989	0.789	1.681
	2	1.0	1.991	0.789	1.683
	3	1.0	1.987	0.788	1.682
	4	1.0	1.043	0.986	1.029
5	1	1.0	1.044	0.985	1.029
	2	1.0	1.991	0.641	1.597
	3	1.0	1.989	0.642	1.596
	4	1.0	1.987	0.642	1.593
6	1	1.0	1.989	0.362	0.664
	2	1.0	1.989	0.365	0.666
	3	1.0	1.989	0.364	0.665
	4	1.0	1.033	0.967	0.989
7	1	1.0	1.049	0.967	0.984
	2	1.0	1.984	0.310	0.575
	3	1.0	1.989	0.313	0.574
	4	1.0	1.989	0.311	0.577
8	1	1.0	1.992	0.261	0.499
	2	1.0	1.991	0.262	0.500
	3	1.0	1.991	0.259	0.498
	4	1.0	1.041	0.959	0.973

[a]As measured by SBRS in 1993.

ing the prelaunch gain calibration of the instrument, calibration pulse data were collected for 120 scans (20 seconds of data collection) for each gain setting and TDI mode. The calibration pulse is observed for 130 pixels of a scan, with a stable plateau in the central 80 pixels of this region. The data analysis used the central 60 pixels of data for each scan to ensure a uniform signal, so the prelaunch gain ratios were computed for 7200 pixels of data.

The gain ratios were first measured in 1993 by the instrument builder, Santa Barbara Remote Sensing (SBRS), during the initial prelaunch calibration of SeaWiFS. Those ratios (from the SeaWiFS Calibration and Data Acceptance Package, prepared by SBRS for NASA) are shown in Table 4. The gain ratios were measured again in 1997 by the National Institute of Standards and Technology (NIST) during the second prelaunch calibration of the instrument. The NIST gain ratios, computed by the OBPG Cal/Val Team, are shown in Table 5 [10]. This table includes an error analysis that was not provided for the SBRS data. Comparison of the two sets of prelaunch data shows that gain ratios remained constant, to within the uncertainties of the second data set, between the 1993 and 1997 calibrations.

3. On-Orbit Gain Calibrations

The first on-orbit calibration method to allow the application of lunar calibrations to Earth observations is to monitor the temporal stability of the gain ratios for each band. To implement this method, the Cal/Val Team has undertaken an analysis of the mission-long time series of 3400 daily gain calibrations, spanning some 3500 days from the start of on-orbit operations in September 1997 through May 2007. This analysis compares the mean gain ratios computed over the mission with the prelaunch values and examines the gain ratio time series for possible trends. The reference time for the time series is the time of the first SeaWiFS on-orbit image, 16 hours 30 minutes UT on 4 September 1997.

Each on-orbit gain calibration cycles through the gain sequence (1, 2, 1, 3, 1, 4, 1) twice for each TDI

Table 5. SeaWiFS Prelaunch Gain Ratios[a]

Band	Detector	GR1	GR2	σ(%)	GR3	σ(%)	GR4	σ(%)
1	1	1.0	1.0156	0.27	1.0051	0.29	1.0105	0.27
	2	1.0	1.9865	0.20	1.3228	0.21	1.6818	0.20
	3	1.0	1.9862	0.21	1.3201	0.21	1.6806	0.21
	4	1.0	1.9925	0.18	1.3194	0.18	1.6796	0.18
2	1	1.0	1.9916	0.16	1.3192	0.16	1.6819	0.16
	2	1.0	1.9841	0.15	1.3189	0.18	1.6810	0.16
	3	1.0	1.9889	0.17	1.3172	0.18	1.6828	0.17
	4	1.0	1.0242	0.46	1.0081	0.47	1.0161	0.46
3	1	1.0	1.0509	0.67	0.9999	0.66	1.0309	0.88
	2	1.0	1.9887	0.17	0.8949	0.17	1.6811	0.17
	3	1.0	1.9886	0.13	0.8968	0.13	1.6811	0.14
	4	1.0	1.9901	0.14	0.8957	0.16	1.6799	0.14
4	1	1.0	1.9901	0.15	0.7869	0.23	1.6814	0.15
	2	1.0	1.9878	0.15	0.7883	0.19	1.6818	0.15
	3	1.0	1.9882	0.15	0.7882	0.16	1.6836	0.15
	4	1.0	1.0435	0.82	0.9855	0.84	1.0290	0.83
5	1	1.0	1.0441	0.83	0.9853	0.86	1.0294	0.84
	2	1.0	1.9908	0.17	0.6414	0.18	1.5964	0.17
	3	1.0	1.9894	0.16	0.6431	0.25	1.5964	0.17
	4	1.0	1.9895	0.15	0.6419	0.16	1.5942	0.15
6	1	1.0	1.9910	0.19	0.3630	0.24	0.6629	0.28
	2	1.0	1.9876	0.21	0.3649	0.31	0.6650	0.27
	3	1.0	1.9905	0.19	0.3642	0.26	0.6652	0.25
	4	1.0	1.0333	0.63	0.9667	0.56	0.9794	0.69
7	1	1.0	1.0492	0.92	0.9666	0.89	0.9682	0.92
	2	1.0	1.9879	0.19	0.3101	0.28	0.5755	0.23
	3	1.0	1.9886	0.17	0.3130	0.32	0.5758	0.29
	4	1.0	1.9905	0.18	0.3109	0.32	0.5769	0.28
8	1	1.0	1.9917	0.17	0.2603	0.46	0.4989	0.21
	2	1.0	1.9891	0.18	0.2613	0.40	0.4995	0.20
	3	1.0	1.9913	0.18	0.2600	0.48	0.4982	0.22
	4	1.0	1.0411	0.78	0.9589	0.81	0.9726	0.80

[a]As measured by NIST in 1997.

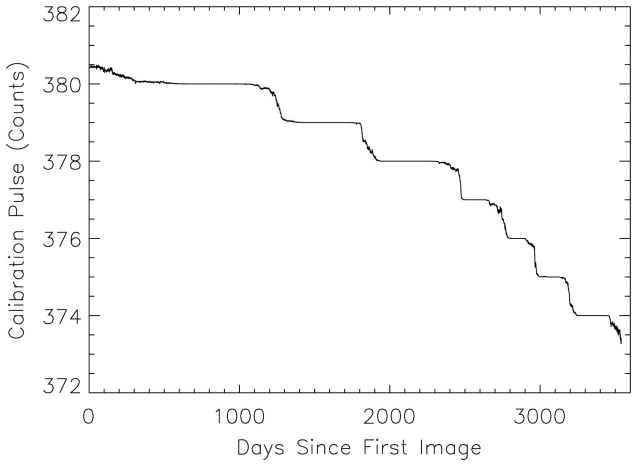

Fig. 4. Band 2 calibration pulse time series. Band 2 shows the greatest change in the calibration pulse over the mission. The data are for the standard gain.

mode (0, 1, 2, 3, 4) [11] to collect gain data for each detector and for the ensemble of detectors in each band. For each gain and TDI setting, calibration pulse data are collected for six scans (1 second of data collection). As with the prelaunch data, the on-orbit data analysis uses the central 60 pixels of data for each scan to ensure a uniform signal. Data are collected twice for each setting, so the daily on-orbit gain ratios are computed for 720 pixels of data. Table 3 shows that the change in the calibration pulse over the 9+ year mission is typically a decrease of 1.5%. Again, the gain ratio computations only require stability over a single gain calibration. Figure 4 shows the mission-long time series for the band 2 calibration pulse at Gain 1, which shows a typical change over the mission.

The close agreement between the prelaunch and on-orbit gain ratios, as provided in Table 6, shows the relative stability of the instrument on orbit. Examination of the ratios shows that the low-gain cloud detectors have larger uncertainties than do the ocean detectors and that the agreement between the prelaunch and on-orbit ratios, particularly for the NIST and on-orbit ratios, is lower for the cloud detectors. The smaller errors for the on-orbit gain ratios compared to the NIST prelaunch ratios are due to the

Table 6. SeaWiFS On-Orbit Gain Ratios[a]

Band	Detector	GR1	GR2	σ(%)	GR3	σ(%)	GR4	σ(%)
1	1	1.0	1.0162	0.091	1.0051	0.027	1.0111	0.11
	2	1.0	1.9879	0.042	1.3231	0.046	1.6823	0.043
	3	1.0	1.9869	0.042	1.3199	0.044	1.6806	0.044
	4	1.0	1.9922	0.037	1.3189	0.039	1.6794	0.034
2	1	1.0	1.9932	0.045	1.3195	0.047	1.6822	0.042
	2	1.0	1.9857	0.035	1.3189	0.043	1.6814	0.041
	3	1.0	1.9895	0.039	1.3179	0.033	1.6826	0.034
	4	1.0	1.0251	0.19	1.0075	0.15	1.0169	0.18
3	1	1.0	1.0418	0.47	0.9922	0.57	1.0267	0.30
	2	1.0	1.9904	0.049	0.8954	0.052	1.6820	0.051
	3	1.0	1.9901	0.039	0.8973	0.069	1.6822	0.043
	4	1.0	1.9909	0.040	0.8959	0.059	1.6805	0.034
4	1	1.0	1.9915	0.051	0.7871	0.078	1.6818	0.052
	2	1.0	1.9888	0.047	0.7880	0.072	1.6819	0.047
	3	1.0	1.9892	0.048	0.7884	0.075	1.6836	0.049
	4	1.0	1.0447	0.29	0.9897	0.63	1.0305	0.37
5	1	1.0	1.0423	0.44	0.9851	0.095	1.0267	0.52
	2	1.0	1.9917	0.049	0.6420	0.077	1.5966	0.046
	3	1.0	1.9900	0.044	0.6425	0.089	1.5965	0.042
	4	1.0	1.9904	0.039	0.6420	0.072	1.5947	0.039
6	1	1.0	1.9918	0.044	0.3633	0.096	0.6627	0.069
	2	1.0	1.9883	0.046	0.3646	0.12	0.6653	0.070
	3	1.0	1.9916	0.046	0.3639	0.13	0.6651	0.063
	4	1.0	1.0376	0.51	0.9724	0.54	0.9842	0.49
7	1	1.0	1.0549	0.73	0.9585	0.72	0.9737	0.79
	2	1.0	1.9893	0.043	0.3100	0.16	0.5758	0.085
	3	1.0	1.9898	0.043	0.3123	0.21	0.5757	0.073
	4	1.0	1.9913	0.036	0.3114	0.12	0.5761	0.093
8	1	1.0	1.9923	0.042	0.2601	0.11	0.4984	0.097
	2	1.0	1.9899	0.037	0.2611	0.27	0.4993	0.073
	3	1.0	1.9926	0.043	0.2596	0.15	0.4987	0.063
	4	1.0	1.0421	0.18	0.9664	0.65	0.9802	0.65

[a]Computed from the mission-long time series.

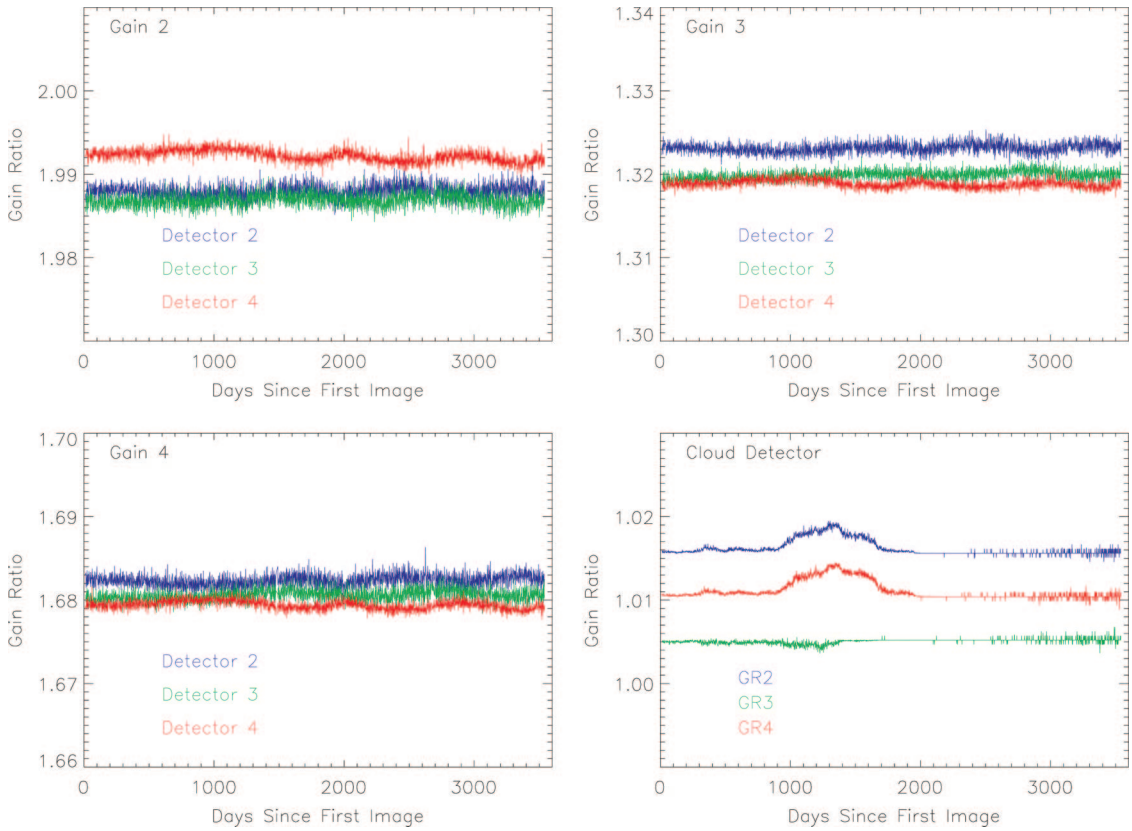

Fig. 5. Gain ratio time series for band 1. The ratios are to the standard gain. The ocean detector ratios are plotted separately for GR2, GR3, and GR4. The cloud detector ratios are plotted together.

larger number of pixels used to compute on-orbit ratios (720 pixels × 3400 calibrations versus 7200 pixels). The time series of gain ratios for band 1 are shown in Fig. 5. Gain 3 and Gain 4 for band 1 are used in the solar and lunar calibrations, respectively. The gains for the cloud detectors do not change. The gain ratio time series for band 1 are typical of the time series for bands 2–8. Gain 3 is the only gain other than Gain 1 that is used in the lunar and solar calibrations for bands 2–8. Accordingly, the time series of GR3 are shown in Fig. 6. For all eight bands, the gain ratios for the ocean detectors are stable to within 0.1% (one calibration pulse count) over the course of the mission.

The on-orbit Earth observations and lunar and solar calibration data are collected using the combined output of the ocean and cloud detectors (the 4:1 TDI mode), so the gain ratios that affect application of the on-orbit instrument calibration to the Earth observations are those for the 4:1 mode. The gain ratios for the 4:1 TDI mode, computed both prelaunch and on-orbit, are shown in Table 7, along with the change in the gain ratios for the lunar gains over the mission. The time series of gain ratios for the 4:1 TDI mode for each band at the lunar calibration gains are shown in Fig. 7. For bands 1–6, the gain ratios change less than 0.1% over the mission, and the changes in the ratios are less than the uncertainties in the means. Such small changes in the gain ratios would have a negligible effect on the Earth observations. For band 7 the gain ratio decreases by 0.76% over the mission, and for band 8 the gain ratio increases by 0.56% over the mission. For both of these bands, the changes in the ratios are larger than the uncertainties in the means. The significance of the change in the gain ratios for bands 7 and 8 is difficult to determine from the gain calibration data alone. Consequently, the Cal/Val Team has looked to a time series of 8-day composite global mean ocean color data products to assess the effect of the gain ratio drifts on the Earth observations [12]. This assessment is discussed in the next section.

4. Application to Ocean Data

The SeaWiFS atmospheric correction algorithm uses the ratio of aerosol radiances in the near-infrared (NIR) bands, band 7 (765 nm) and band 8 (865 nm), to propagate the observed aerosol radiances from the NIR bands to the visible bands [13]. This ratio is characterized by the parameter ϵ:

$$\epsilon(\lambda,\ 865) = \frac{L_{as}(\lambda)F_0(865)}{L_{as}(865)F_0(\lambda)}. \tag{2}$$

Here, L_{as} is the single-scattering aerosol radiance and F_0 is the solar constant. In the atmospheric correction

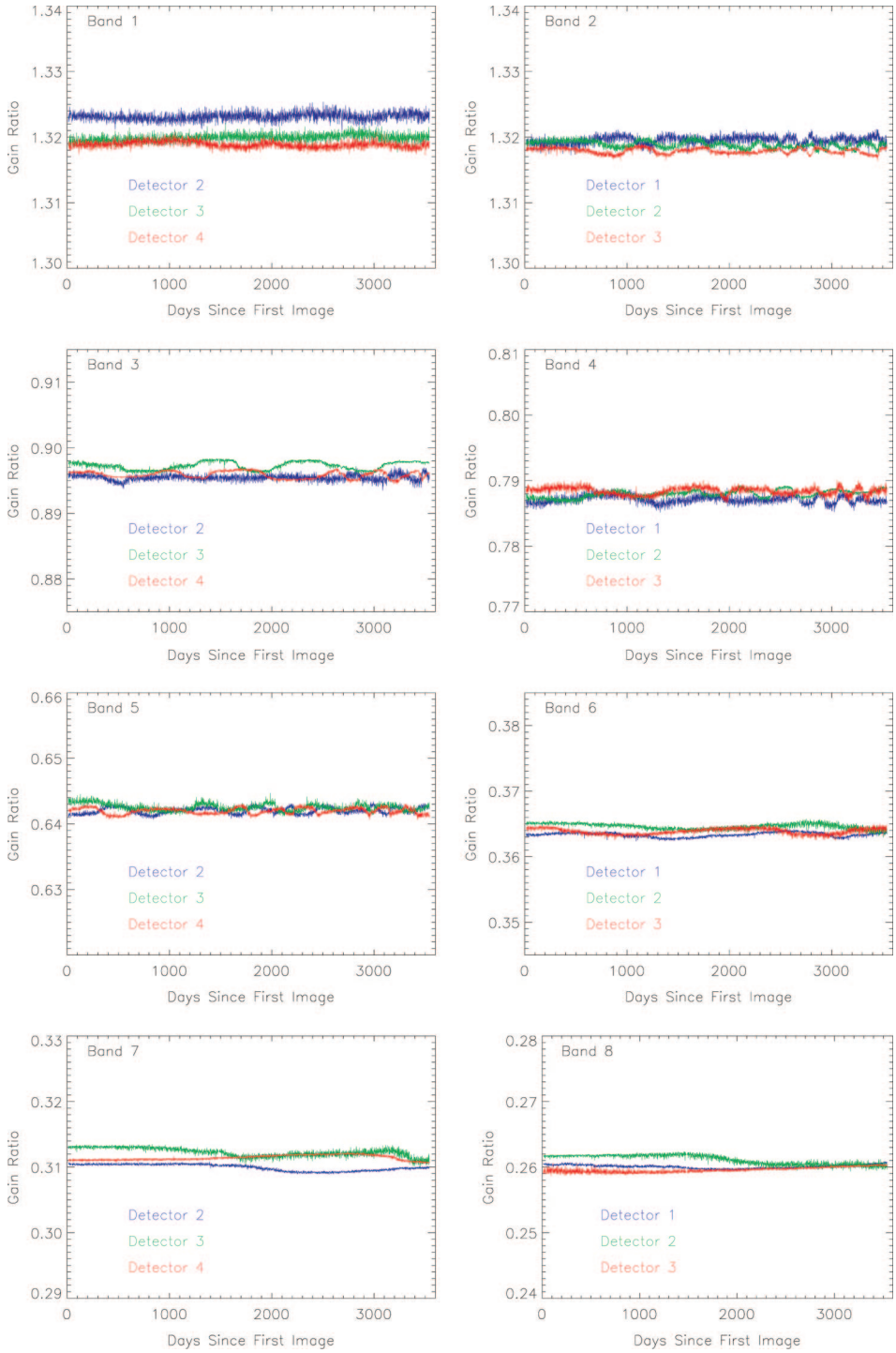

Fig. 6. Ocean detector GR3 time series for all bands. The ratios are to the standard gain.

algorithm, ϵ is evaluated for band 7 and then used to extrapolate the aerosol radiance at band 8 to the visible bands (bands 1–6). An alternate parameterization of the atmospheric correction is the angstrom exponent α:

$$\alpha(\lambda) = \log_e\left(\frac{\tau_a(\lambda)}{\tau_a(865)}\right)\Big/\log_e\left(\frac{865}{\lambda}\right). \tag{3}$$

Here τ_a is the aerosol optical depth. In the atmospheric correction algorithm, α is dependent on the band 7 to band 8 radiance ratio. Any drifts in ϵ over the mission would propagate through the atmospheric correction algorithm into the water-leaving radiance and chlorophyll retrievals. Because of the sensitivity of the ϵ, water-leaving radiance, and chlorophyll retrievals to small changes in the instrument calibration [3], the Cal/Val Team has used the mission-long time series of

Table 7. SeaWiFS Gain Ratios for the 4:1 TDI Mode[a]

Band	Ratio	SBRS	NIST	σ(%)	On Orbit	σ(%)	Δ(%)
1	GR1	1.0	1.0		1.0		
	GR2	1.931	1.8686	0.20	1.8677	0.047	
	GR3	1.302	1.2817	0.18	1.2809	0.065	
	GR4	1.642	1.5987	0.20	1.5974	0.061	−0.100
2	GR1	1.0	1.0		1.0		
	GR2	1.940	1.9076	0.18	1.9095	0.054	
	GR3	1.303	1.2917	0.11	1.2921	0.057	−0.048
	GR4	1.648	1.6268	0.13	1.6275	0.060	
3	GR1	1.0	1.0		1.0		
	GR2	1.951	1.9385	0.33	1.9410	0.068	
	GR3	0.900	0.9003	0.19	0.9011	0.068	+0.029
	GR4	1.655	1.6467	0.30	1.6483	0.070	
4	GR1	1.0	1.0		1.0		
	GR2	1.955	1.9423	0.027	1.9439	0.059	
	GR3	0.796	0.7967	0.025	0.7976	0.11	−0.037
	GR4	1.658	1.6506	0.11	1.6508	0.074	
5	GR1	1.0	1.0		1.0		
	GR2	1.961	1.9464	0.19	1.9473	0.061	
	GR3	0.652	0.6572	0.12	0.6581	0.11	+0.079
	GR4	1.579	1.5696	0.17	1.5702	0.064	
6	GR1	1.0	1.0		1.0		
	GR2	1.969	1.9292	0.24	1.9304	0.051	
	GR3	0.376	0.4006	0.032	0.4016	0.16	+0.071
	GR4	0.671	0.6843	0.14	0.6846	0.089	
7	GR1	1.0	1.0		1.0		
	GR2	1.969	1.9514	0.18	1.9506	0.055	
	GR3	0.323	0.3412	0.12	0.3395	0.26	−0.761
	GR4	0.583	0.5926	0.059	0.5930	0.10	
8	GR1	1.0	1.0		1.0		
	GR2	1.975	1.9429	0.29	1.9449	0.048	
	GR3	0.272	0.2933	0.055	0.2943	0.18	+0.562
	GR4	0.507	0.5213	0.17	0.5211	0.15	

[a]σ are standard deviations of the means. Δ are changes in the lunar gain ratios over the mission.

the 8-day global mean values as diagnostic tools to assess the effect of the gain ratio drifts in the NIR bands on the ocean observations.

A. Ocean Data Anomaly Analysis

This analysis examines long-term trends in the level 3 ocean color products (water-leaving radiances for bands 1–6, chlorophyll, and ϵ) and the consistency of those trends from year to year. It provides a standard mechanism for evaluating derived product and sensor stability, and it quantifies the relative effect of calibration and algorithm changes on global spatial scales and life-of-mission time scales. The approach begins with the level 3 products. These products are global binned, multiday averages at 9 km resolution, with bins distributed in an equal-area, sinusoidal projection. The typical composite period is 8 days, but for quick turnaround test processing the Cal/Val Team uses a temporal subset of the mission lifespan consisting of 4 day composites generated from the start of each consecutive 32 day period. The temporal subset is generated at 9 km resolution, and it can be processed within one day. The 4 day compositing period generally provides sufficient opportunity to observe most of the daylit side of the Earth, including coverage in orbit and glint gaps. From these global, multiday composites, a subset of the filled bins is selected, and the ocean products are averaged and trended with time. For the analysis reported here, the Cal/lVal Team uses a global deep water data subset, which consists of all bins where water depth is greater than 1000 meters. Annual climatologies are computed for the ocean products for both the 8 day and 4 day time series, using the 9+ year-long mission data set. Anomaly plots are then generated for each product, where the anomaly is defined as the long-term trend with the annual climatology subtracted. In this analysis, 114 composites are used that span the time range of November 1997 through May 2007.

The initial set of anomaly plots for the deepwater subset of the level 3 ocean color products is shown in Fig. 8 and Fig. 9. These plots show normalized water-leaving radiances (L_{WN}) for bands 1–6 (412 nm,

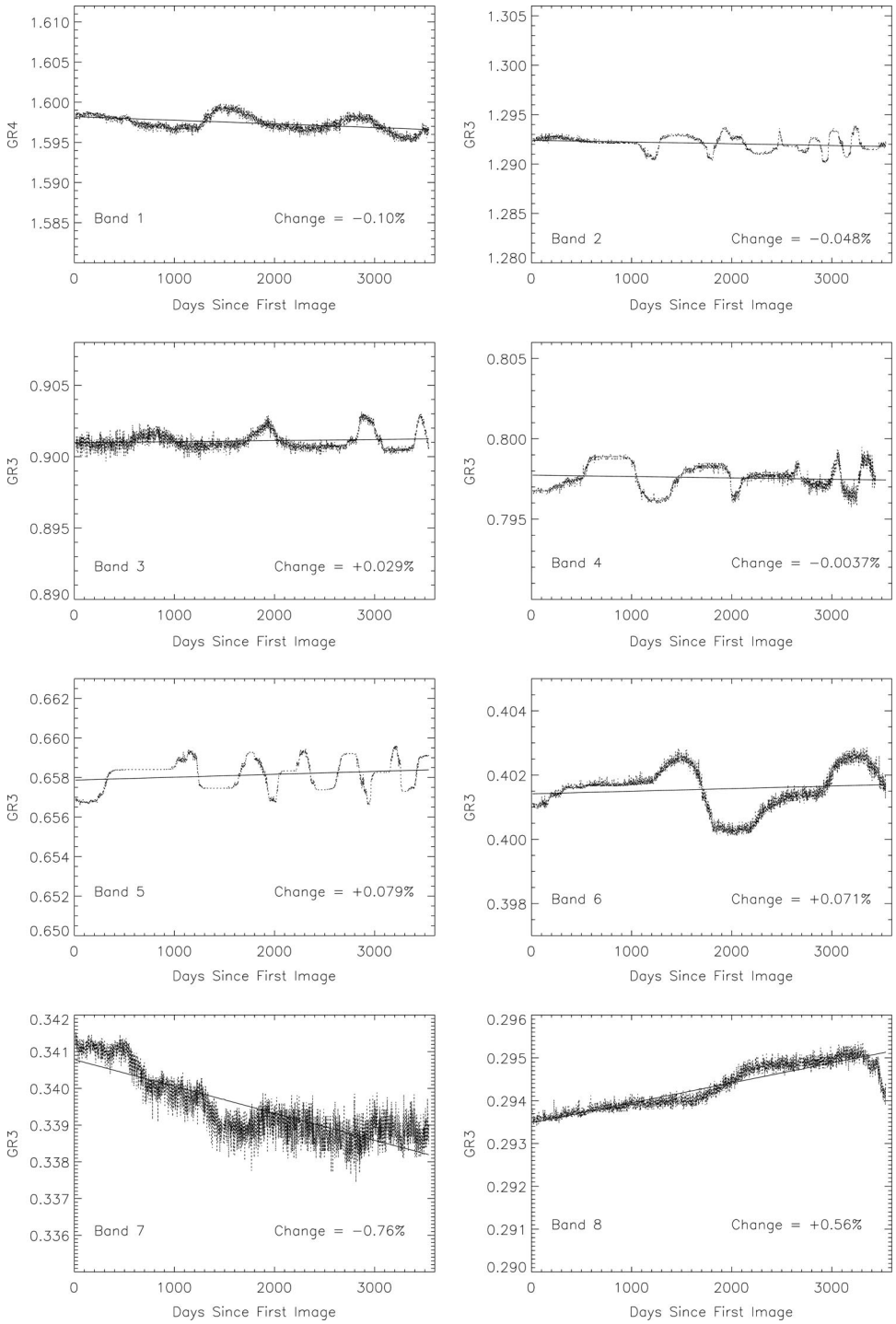

Fig. 7. Gain ratio time series for the 4:1 TDI mode for all bands. The ratios are to the standard gain. The linear fits show the changes over the mission.

443 nm, 490 nm, 510 nm, 555 nm, and 670 nm), chlorophyll, and ϵ, along with linear trends fit to each time series. Examination of these plots shows that it is often difficult to distinguish between secular trends in the data, interannual effects (e.g., the El Nino Southern Oscillation), and possible drifts in the instrument calibration. The anomaly plot for $L_{\mathrm{WN}}(510)$ should not show any trends for the deepwater ocean, even in the presence of secular trends in chlorophyll or aerosols. However, this plot does show an unexplained decrease of 0.020 mW cm^{-2} sr^{-1} μm^{-1} in this band over the mission (a 2.9% change), with an accompanying increase for ϵ of 0.030 over the mission (a 2.8% change). This trend in ϵ has been reported by Wang *et al.* [14] as a trend in the angstrom exponent and has been ascribed by them to uncorrected drifts in the calibration of bands 7 and 8. The Cal/Val Team proceeded to investigate any correlation between the

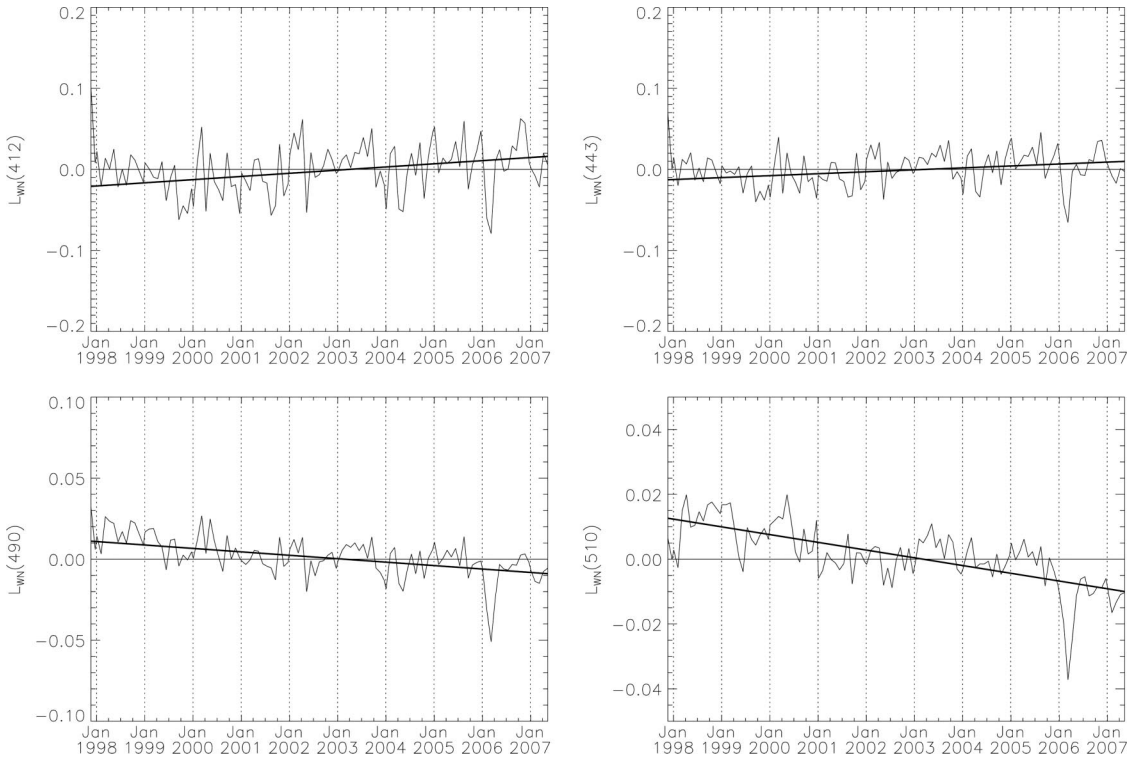

Fig. 8. Level 3 time series anomaly plots. These plots show L_{WN} for bands 1–4 (412 nm, 443 nm, 490 nm, 510 nm). The linear fits show the trends over the mission. The radiance units are mW cm^{-2} sr^{-1} μm^{-1}.

trends in $L_{WN}(510)$ and ϵ and the NIR band gain ratio drifts.

As shown in Fig. 7 and Table 7, GR3 for the NIR bands change -0.76% (765 nm) and $+56\%$ (865 nm) over the mission. The effect of these drifts on the ocean products comes through the NIR band ratio, which is plotted in Fig. 10. The drift in the band ratios over the mission is -1.3%, which is comparable to the drift in $L_{WN}(510)$ and ϵ. In order to correct the calibration of the instrument for gain ratio drift, the Cal/Val Team has computed a series of piecewise linear fits to GR3 for bands 7 and 8, as shown in Fig. 11. These fits have been used to correct the lunar calibration time series for the drift. The Cal/Val Team then recomputed the change in the radiometric response of the instrument over time for these two bands and generated a revised SeaWiFS calibration table.

B. Assessment of GR3 Drift Correction

As a first assessment of the GR3 drift correction on the ocean products, the Cal/Val Team examined changes in the vicarious calibration of SeaWiFS. The vicarious calibration adjusts the integrated instrument and atmospheric correction algorithm system to retrieve normalized water-leaving radiances that are in agreement with ground truth measurements using data from the Marine Optical Buoy (MOBY) and observations of clear-water sites in the South Pacific and southern Indian Ocean [4,5]. The calibration produces a set of multiplicative gains for the top-of-atmosphere (TOA) radiances in each band that are independent of time and location. For the NIR bands, the Cal/Val Team assumes that the vicarious gain of the 865 nm band is unity and adjusts the gain of the 765 nm band so that the atmospheric correction algorithm retrieves the expected aerosol models for selected open-ocean scenes. The Cal/Val Team then adjusts the vicarious gains of the visible bands to match the L_{WN} measured by MOBY. The comparison of the vicarious gains for SeaWiFS before and after the GR3 drift correction are shown in Table 8. Changing the gain of band 8 causes a change in the total aerosol radiance retrieved by the atmospheric correction algorithm, since the vicarious gain for band 8 is unity. Changing the gains of bands 7 and 8 causes a change of almost 0.3% in the vicarious calibration of band 7. For the visible bands, changes in the total aerosol radiance would have a larger effect in the green bands than the blue bands, since the aerosol radiance is a larger component of the TOA radiance for the green bands. Consequently, changing the gains of the NIR bands together propagates into a steadily decreasing effect with shorter wavelength in the vicarious calibration of the visible bands.

The mission-long ocean color test data set has been reprocessed with the revised temporal corrections for the NIR bands. The revised anomaly plots are shown in Fig. 12 and Fig. 13. The drift in $L_{WN}(510)$ has essentially been eliminated, and the drift in ϵ has been reduced to 0.021 (2.0% over the mission). The changes in L_{WN} for the other bands and in the chlorophyll are of the expected magnitude arising from the change in ϵ. The source of the residual trend in ϵ

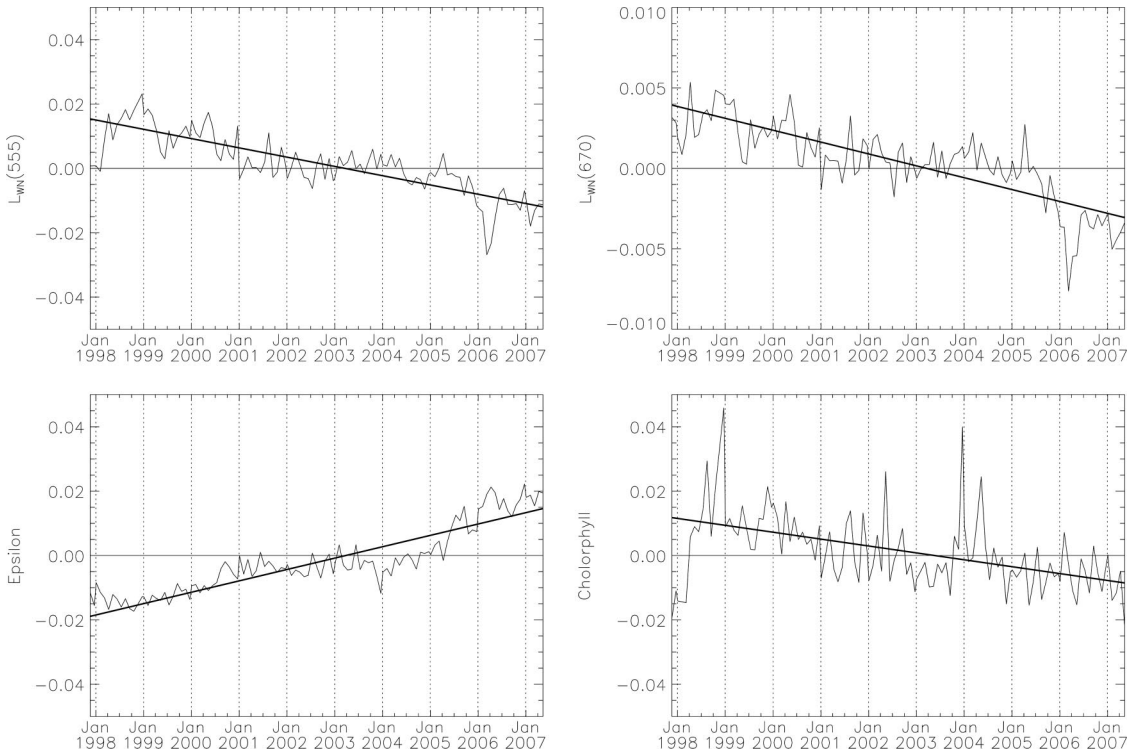

Fig. 9. Level 3 time series anomaly plots. These plots show L_{WN} for band 5 (555 nm), band 6 (670 nm), epsilon, and chlorophyll. The linear fits show the trends over the mission. The radiance units are mW cm^{-2} sr^{-1} μm^{-1}, epsilon is dimensionless, and the chlorophyll units are mg m^{-3}.

may be due to changing aerosol concentration in the atmosphere over the mission, as is suggested by Fukushima *et al.* [15] for East Asia, though the global extent of such changes have not been verified [14]. This analysis shows the sensitivity of ocean color data to small drifts in the instrument calibration over time and demonstrates the use of time series of global mean products to monitor changes in the instrument response. The update to SeaWiFS calibration to correct for the GR3 drift in the NIR bands will be incorporated into the next reprocessing of the SeaWiFS mission-long ocean data set. By making the GR3 drift correction for the NIR bands, the Cal/Val Team will maintain the validity of applying changes in the radiometric response of SeaWiFS derived from lunar data obtained at the lunar commanded gains to ocean data obtained at the standard gains.

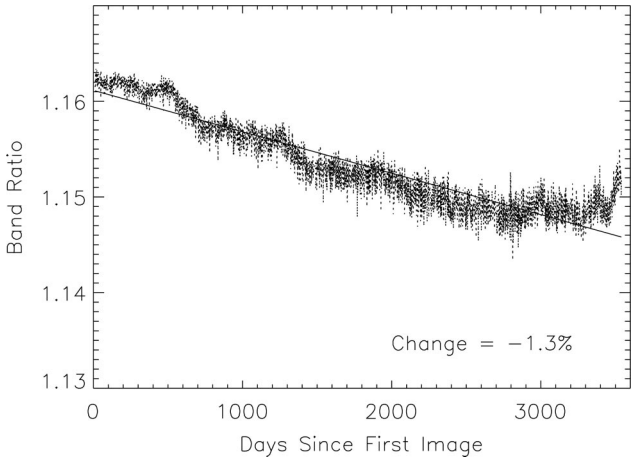

Fig. 10. Band 7/band 8 ratio. The linear fit shows the change in the band ratio over the mission due to the GR3 drift.

5. On-Orbit Detector Calibrations

The second on-orbit calibration method to allow the application of lunar calibrations to Earth observations is to monitor the radiometric stability of the detectors in each band. To implement this method, the Cal/Val Team has undertaken an analysis of the mission-long time series of 3300 daily detector calibrations, spanning some 3500 days from the start of on-orbit operations in September 1997 through May 2007. The on-orbit detector calibrations are solar calibrations that have been modified to collect data from each detector individually during the solar measurements. The detector calibrations monitor the variations in the radiometric response of the individual detectors with respect to the ensemble of detectors in each band by computing the ratios of the solar calibration time series for each detector to the solar calibration time series for the 4:1 TDI mode. This section discusses solar calibrations in the context of the detector calibrations. A more detailed discussion of SeaWiFS on-orbit solar calibrations is provided by Eplee *et al.* [16]. Again, the reference time for the observations is the time of the first SeaWiFS on-orbit image, 16 hours 30 minutes UT on 4 September 1997.

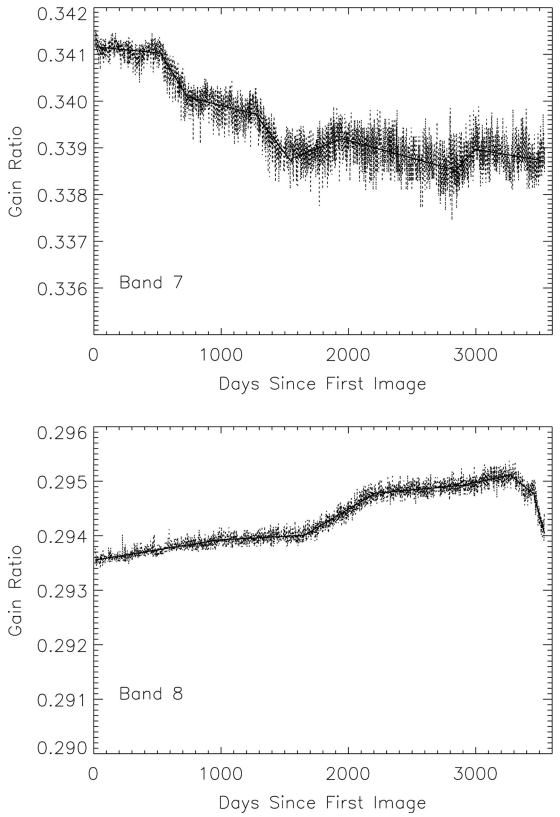

Fig. 11. GR3 time series for bands 7 and 8. The piecewise linear corrections to the lunar calibration time series are shown.

Each on-orbit detector calibration cycles through the TDI sequence (0, 1, 0, 2, 0, 3, 0, 4) ten times [11], where 0 is the 4:1 mode. For each TDI setting, solar calibration data are collected for six scans (1 second of data collection). The diffuser is observed for 480 pixels, but the changing illumination of the diffuser by the Sun during the scan limits the useful data to seven pixels centered on the region of maximum illumination. Data are collected ten times for each setting, so the daily on-orbit detector calibrations are computed for 420 pixels of data. The detector calibration time series for all eight bands are shown in Fig. 14. Since the detector calibrations measure radiances reflected from the solar diffuser, the time series are plotted in terms of the measured radiances normalized to the first observation for each detector. The data studied in this analysis have been calibrated with the prelaunch SeaWiFS calibration table, so the data have not been corrected for changes in the radiometric response of the instrument over time. This approach allows the Cal/Val Team to monitor the actual performance of the individual detectors over the mission. Accordingly, these plots show the effects of varying azimuth angles of the solar irradiance, diffuser reflectance degradation, and changes in radiometric response of the instrument over the mission [16]. The primary observation from the examination of these plots is that the radiometric responses of the individual detectors in each band, including the cloud detectors, closely track each other.

Table 8. Vicarious Gains for SeaWiFS[a]

Band	Wavelength	Gain before Correction	Gain after Correction	Δ(%)
1	412	1.0367	1.0368	0.0096
2	443	1.0128	1.0129	0.0099
3	490	0.9913	0.9914	0.010
4	510	0.9975	0.9978	0.030
5	555	0.9987	0.9989	0.020
6	670	0.9724	0.9728	0.041
7	765	0.9691	0.9717	0.27
8	865	1.00	1.00	

[a]Δ are the change in the gains due to the GR3 drift corrections.

For the detector calibration data analysis, the Cal/Val Team computes the ratios of the individual detector time series to the time series for the ensemble of detectors (the 4:1 TDI mode):

$$R(\lambda,\ \mathrm{TDI}_i) = \frac{L(\lambda,\ \mathrm{TDI}_i)}{L(\lambda,\ \mathrm{TDI}_{4:1})}. \tag{4}$$

Here, $L(\lambda, \mathrm{TDI}_i)$ is the detector calibration time series for each detector of each band, and $L(\lambda, \mathrm{TDI}_{4:1})$ is the detector calibration time series for the 4:1 TDI mode for that band. The ratio analysis removes most of the effects of the solar azimuth angle variation, the reflectance degradation, and the changing radiometric response, and allows small variations between the individual detectors and the ensemble to be monitored. The normalized detector calibration time series for all eight bands are shown in Fig. 15. The radiometric sensitivity of the cloud detectors is lower than that for the ocean detectors, so the noise for the cloud detectors is higher. Within each band, there are offsets among the detectors that change slowly, if at all, over the mission.

The plots show that the ratio analysis does not fully remove the solar azimuth angle variation from the time series late in the mission, when the effects of drift in the node of the spacecraft orbit become significant [16]. Review of Fig. 2 for the 4:1 TDI mode and the individual detector TDI modes suggests that the differences in the detector response ratios within each band raise differences in the fields of view for data collected in the 4:1 and individual detector TDI modes. For the 4:1 TDI mode, the time delay ensures that the output from each detector originates from the same pixel on the diffuser during the instrument scan. For the individual detector TDI modes, the time delay causes data from four adjacent pixels on the diffuser to be averaged together. The different optical paths beween detectors, the diffuser, and the diffuser aperture screen for data collected in the 4:1 and individual detector TDI modes would give rise to the observed variations in detector response ratios as functions of solar azimuth angle [16,17]. This conclusion

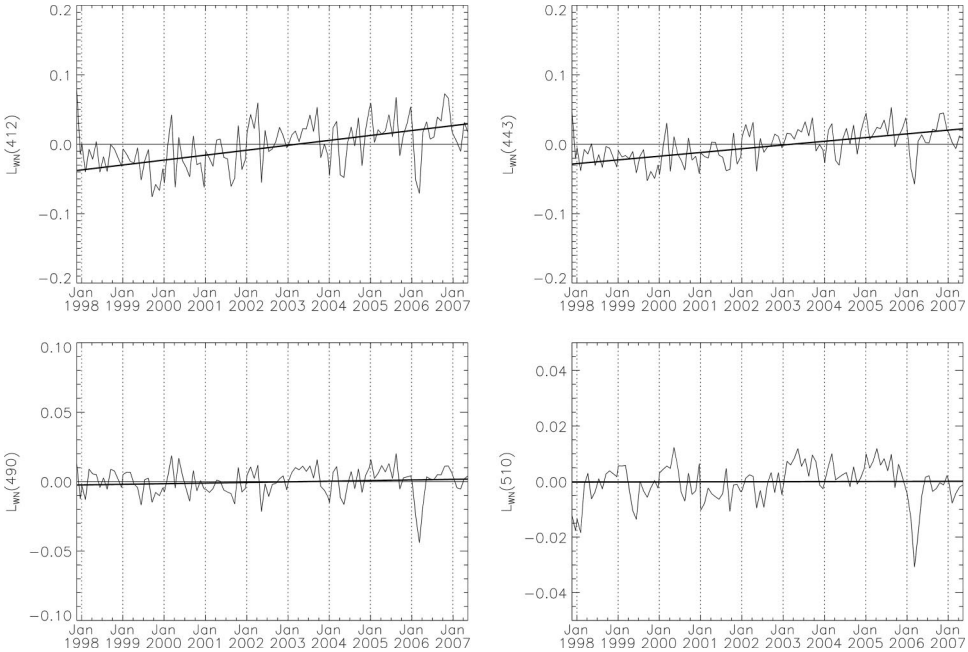

Fig. 12. Level 3 time series anomaly plots after GR3 drift correction. These plots show L_{WN} for bands 1–4 (412 nm, 443 nm, 490 nm, 510 nm). The linear fits show the trends over the mission. The radiance units are mW cm^{-2} sr^{-1} μm^{-1}.

about the late mission behavior is supported by the pronounced residual azimuth angle response of the cloud detectors, the larger residual response observed for the outside detectors compared to the interior detectors within each band, and the larger response observed for the detectors of the even-numbered bands compared to the detectors of the odd-numbered bands within each focal plane. Similar detector-dependent responses to variations in the solar azimuth angles have also been observed for the Moderate Resolution Imaging Spectroradiometer (MODIS) [18,19], though the cause of the variations is different.

The detectors in band 8 show the largest trends over time with respect to the ensemble behavior. Since band 8 shows the largest change in radiometric response over the mission, small variations in the response of the individual detectors would give

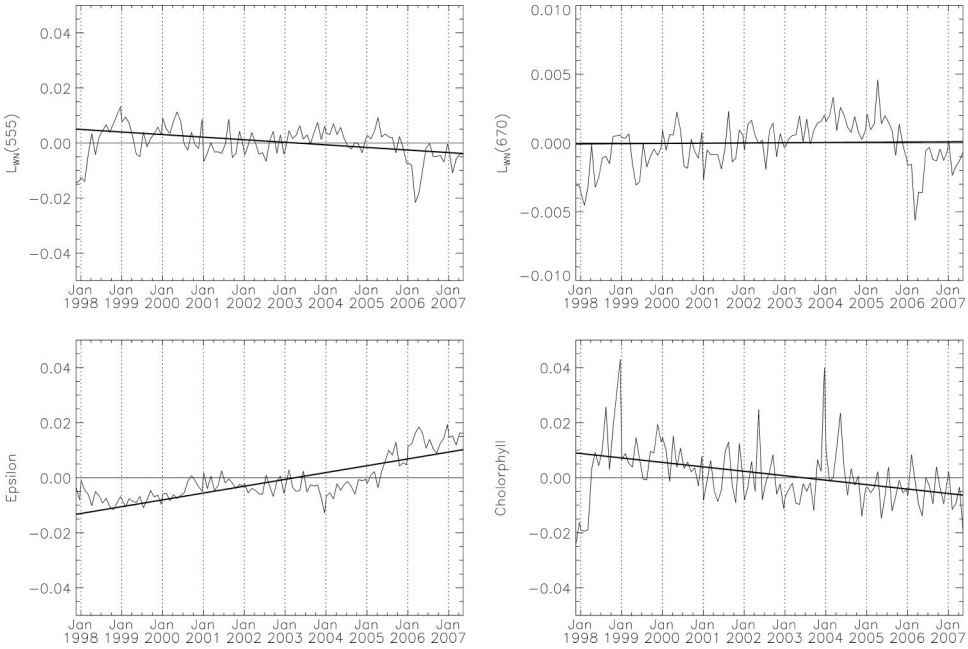

Fig. 13. Level 3 time series anomaly plots after GR3 drift correction. These plots show L_{WN} for band 5 (555 nm), band 6 (670 nm), epsilon, and chlorophyll. The linear fits show the trends over the mission. The radiance units are mW cm^{-2} sr^{-1} μm^{-1}, epsilon is dimensionless, and the chlorophyll units are mg m^{-3}.

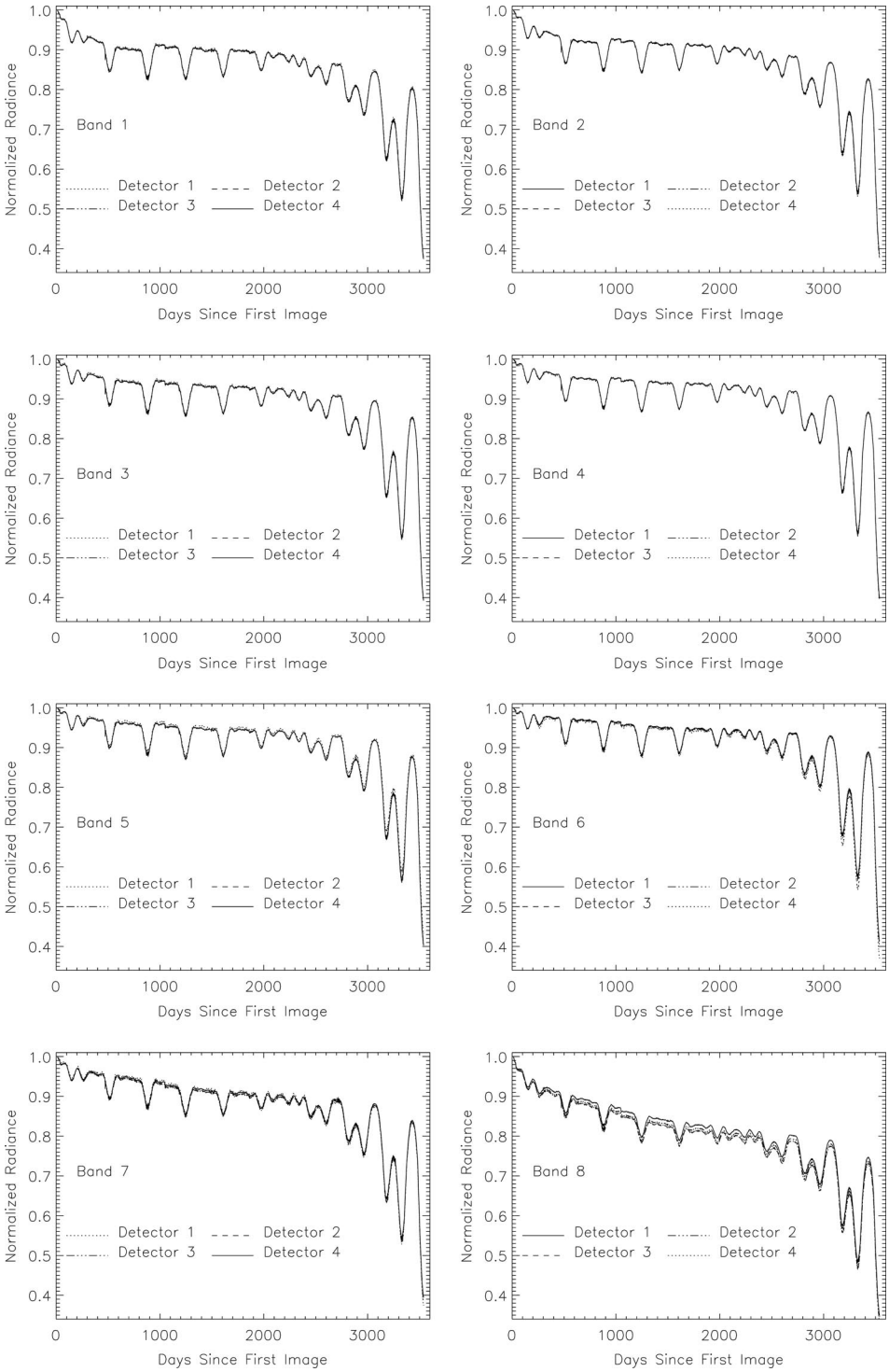

Fig. 14. Detector calibration time series. For each detector, the time series are normalized to the first observation. The cloud detectors are detector 1 for the odd-numbered bands and detector 4 for the even-numbered bands.

rise to the observed trends. The time series are continuous for all bands and detectors, except for the cloud detector in band 7. This detector shows a one count step function some 2700 days into the mission (approximately 1 January 2005). The 4:1 TDI mode reduces this step function to 1/4 count. The change in cloud detector for band 7 does not affect the performance of the atmospheric correction algorithm because of the small effect of a 1/4 count change below the knee of the bilinear response. For bands 1–7, the variations in the response of the individual detectors from the response of the ensemble is less than 0.5% over the mission. For band 8 the variations are less than 1%. For all eight bands, the

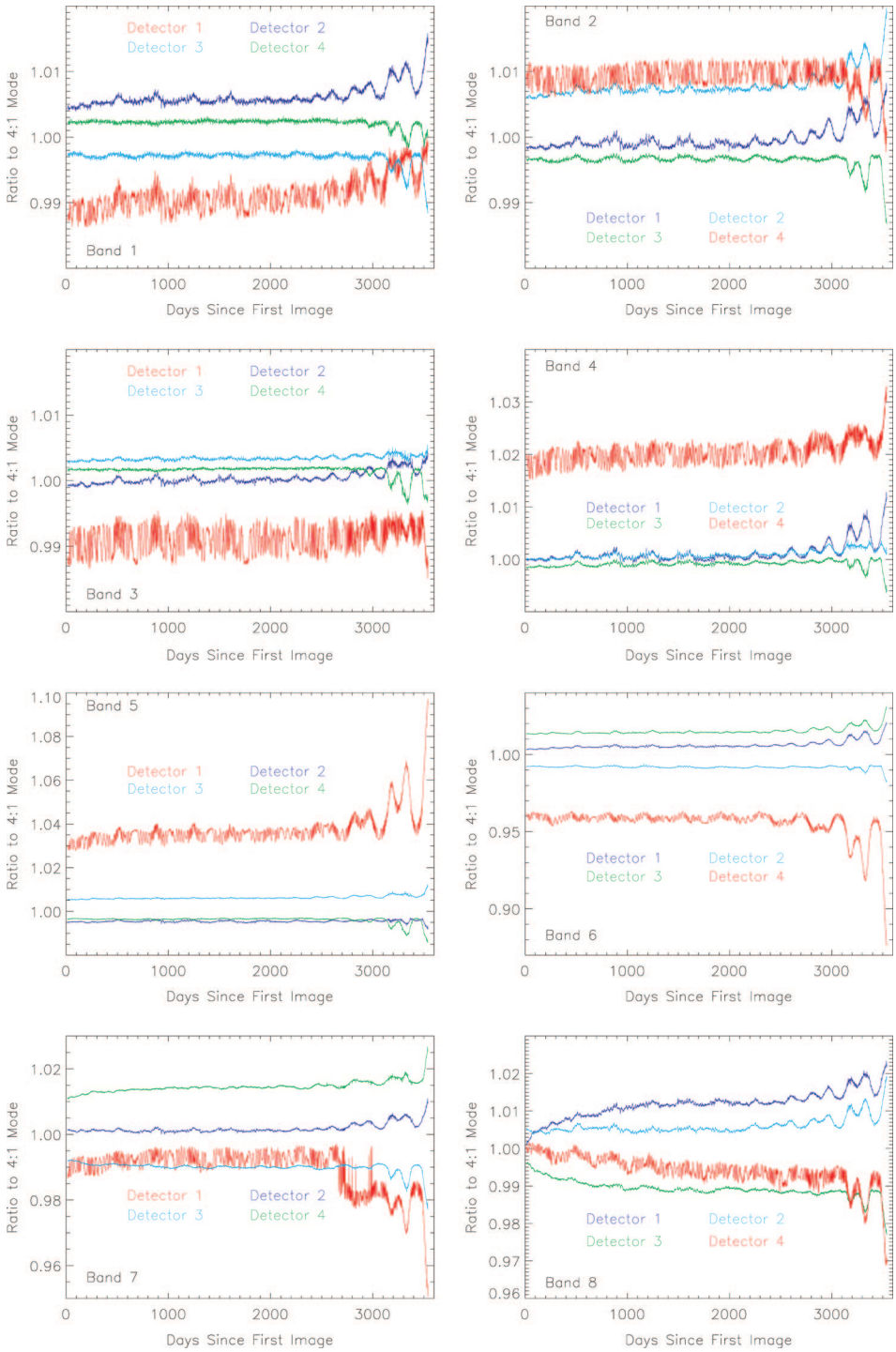

Fig. 15. Normalized detector calibration time series. For each band, the individual detector time series are normalized to the time series for the ensemble (the 4:1 TDI mode). The cloud detectors are shown in red.

cloud detectors do not show any systematic differences from the ocean detectors. Consequently, the changes in the radiometric response of the instrument derived from lunar calibration data obtained with all four detectors in each band (below the knee of the bilinear response) can be applied to the cloud detector alone (above the knee of the bilinear response). The radiometric corrections for clouds, photosynthetically active radiation (PAR), normalized difference vegetation index (NDVI), and land surface reflectances are valid.

6. Discussion

Since SeaWiFS has almost completed the tenth year of its mission, analysis of its on-orbit calibration data provides a unique opportunity to study long-term trends in the radiometric performance of scanning filter radiometers. The OBPG Cal/Val Team, through

its use of mission-long time series of on-orbit gain ratios, ensures that changes in the radiometric response of SeaWiFS derived from lunar data obtained at one set of commanded gains can be applied to ocean data obtained at a different set of gains. The Cal/Val Team, through its use of mission-long detector calibration time series, ensures that changes in the instrument response derived from data obtained with all four detectors in each band (below the knee of the bilinear response) can be applied to the cloud detector alone (above the knee of the bilinear response). While these specific calibration strategies are unique to SeaWiFS, the SeaWiFS experience should influence the development of future ocean color missions.

The SeaWiFS gain calibration experience shows that future missions would benefit by expanding the dynamic range of new instruments to cover both typical radiances for the Earth observations and radiances from the calibration sources (the Moon or solar diffusers). MODIS uses this approach with the limitation that ocean color bands 13–16 (667 nm, 678 nm, 748 nm, and 869 nm) saturate on the Moon. An alternate approach for future missions would be to maintain separate on-orbit calibrations for each instrument gain. Such a calibration strategy is currently under development for the Visible and Infrared Radiometer Suite (VIIRS) on the National Polar-orbiting Operational Environmental Satellite System (NPOESS) and NASA NPOESS Preparatory Project.

This work demonstrates the importance of a mission-long calibration/validation program to the generation and maintenance of a long-term climate quality ocean color data set. Any drifts in the SeaWiFS gain ratios cannot be extracted from the lunar calibration data set, which is the primary monitor of the on-orbit change in radiometric response of the instrument. The on-orbit gain ratio time series derived from the gain calibration data showed drifts for bands 7 and 8. The assessment of the effect of these drifts on the ocean data required the Cal/Val Team to examine the mission-long time series of global means of ocean color data products. This data analysis showed trends that were correlated with the gain drifts and showed, more generally, the sensitivity of ocean color data to small drifts in the instrument calibration over time.

This work shows the necessity of maintaining mission-long time series of global mean data products from Earth-observing sensors to evaluate the derived products and to validate the sensor calibration stability. These time series are sensitive monitors of small changes in the calibration of the instruments on orbit. The OBPG maintains these time series for SeaWiFS and MODIS. Such an approach will be required by the NPOESS Preparatory Project to ensure that climate quality data can be obtained from VIIRS.

References

1. C. R. McClain, W. E. Esaias, W. Barnes, B. Guenther, D. Endres, S. B. Hooker, B. G. Mitchell, and R. Barnes, *SeaWiFS Calibration and Validation Plan,* NASA Tech. Memo. 104566 **3,** S. B. Hooker and E. R. Firestone, eds. (NASA Goddard Space Flight Center, Greenbelt, Maryland, 1992).
2. R. A. Barnes, R. E. Eplee, Jr., F. S. Patt, and C. R. McClain, "Changes in the radiometric stability of SeaWiFS determined from lunar and solar-based measurements," Appl. Opt. **38,** 4649–4664 (1999).
3. R. A. Barnes, R. E. Eplee, Jr., G. M. Schmidt, F. S. Patt, and C. R. McClain, "Calibration of SeaWiFS. I. Direct techniques," Appl. Opt. **40,** 6682–6700 (2001).
4. R. E. Eplee, Jr., W. D. Robinson, S. W. Bailey, D. K. Clark, P. J. Werdell, M. Wang, R. A. Barnes, and C. R. McClain, "Calibration of SeaWiFS. II. Vicarious techniques," Appl. Opt. **40,** 6701–6718 (2001).
5. B. A. Franz, S. W. Bailey, P. J. Werdell, and C. R. McClain, "Sensor-independent approach to the vicarious calibration of satellite ocean color radiometry," Appl. Opt. **46,** 5068–5082 (2007).
6. R. E. Eplee, Jr., R. A. Barnes, and C. R. McClain, "SeaWiFS detector and gain calibrations: four years of on-orbit stability," in *Earth Observing Systems VII,* Proc. SPIE **4814,** 282–288 (2002).
7. R. A. Barnes, A. W. Holmes, W. L. Barnes, W. E. Esaias, C. R. McClain, and T. Svitek, *SeaWiFS Prelaunch Radiometric Calibration and Spectral Characterization,* NASA Tech. Memo. 104566 **23,** S. B. Hooker, E. R. Firestone, and J. G. Acker, eds. (NASA Goddard Space Flight Center, Greenbelt, Maryland, 1994).
8. R. E. Eplee, Jr., R. A. Barnes, F. S. Patt, G. Meister, and C. R. McClain, "SeaWiFS lunar calibration methodology after six years on orbit," in *Earth Observing Systems IX,* Proc. SPIE **5542,** 1–13 (2004).
9. R. E. Eplee, Jr., F. S. Patt, G. Meister, B. A. Franz, S. W. Bailey, and C. R. McClain, "The on-orbit calibration of SeaWiFS: revised temperature and gain corrections," in *Earth Observing Systems XII,* Proc. SPIE **6677,** 667713 (2007).
10. B. C. Johnson, E. E. Early, R. E. Eplee, Jr., R. A. Barnes, and R. T. Caffrey, *The 1997 Prelaunch Radiometric Calibration of SeaWiFS,* NASA Tech. Memo. 1999–206892 **4,** S. B. Hooker and E. R. Firestone, eds. (NASA Goddard Space Flight Center, Greenbelt, Maryland, 1999).
11. R. H. Woodward, R. A. Barnes, C. R. McClain, W. E. Esaias, W. L. Barnes, and A. T. Mecherikunnel, *Modeling of the SeaWiFS Solar and Lunar Calibrations,* NASA Tech. Memo. 104566 **10,** S. B. Hooker and E. R. Firestone, eds. (NASA Goddard Space Flight Center, Greenbelt, Maryland, 1993).
12. B. A. Franz, P. J. Werdell, G. Meister, S. W. Bailey, R. E. Eplee, Jr., G. C. Feldman, E. Kwaitkowska, C. R. McClain, F. S. Patt, and D. Thomas, "The continuity of ocean color measurements from SeaWiFS to MODIS," in *Earth Observing Systems X,* Proc. SPIE **5882,** 58820W (2005).
13. H. R. Gordon and M. Wang, "Retrieval of water-leaving radiance and aerosol optical thickness over the oceans with SeaWiFS—a preliminary algorithm," Appl. Opt. **33,** 443–452 (1994).
14. M. Wang, K. D. Knobelspiesse, and C. R. McClain, "Study of the Sea-Viewing Wide Field-of-View Sensor (SeaWiFS) aerosol optical property data over ocean in combination with the ocean color products," J. Geophys. Res. **110,** D10S06 doi:10.1029/2004JD004950 (2005).
15. H. Fukushima, L.-P. Li, and K. Takeno, "Increasing trend in sub-micron aerosol particles over East Asian waters observed in 1998–2004 by Sea Wide Field-of-View Sensor (SeaWiFS)," in *Remote Sensing of Clouds and the Atmosphere XI,* Proc. SPIE **6362,** 636205 (2006).
16. R. E. Eplee, Jr., F. S. Patt, R. A. Barnes, and C. R. McClain, "SeaWiFS long-term solar diffuser reflectance and sensor noise analyses," Appl. Opt. **46,** 762–773 (2007).

17. R. A. Barnes and R. E. Eplee, Jr., "The SeaWiFS solar diffuser," in *SeaWiFS Calibration Topics, Part 1,* NASA Tech. Memo. 104566 **39,** S. B. Hooker and E. R. Firestone, eds. (NASA Goddard Space Flight Center, Greenbelt, Maryland, 1996), pp. 54–61.
18. X. Xie, X. Xiong, D. Moyer, J. Sun, X. Liu, and W. Barnes, "Analysis of the MODIS solar diffuser screen vignetting function," in *Earth Observing Systems X,* Proc. SPIE **5882,** 58820T (2005).
19. G. Meister, F. S. Patt, X. Xiong, J. Sun, X. Xie, and C. R. McClain, "Residual correlations in the solar diffuser measurements of the MODIS Aqua ocean color bands to the sun yaw angle," in *Earth Observing Systems X,* Proc. SPIE **5882,** 58820V (2005).